Analyst

Analyst

www.rsc.org/analyst

ROYAL SOCIETY OF CHEMISTRY

www.rsc.org/analyst

Analyst

ARTICLE

Label-free imaging and identification of typical cells of acute myeloid leukaemia and myelodysplastic syndrome by Raman microspectroscopy

R. Vanna[a], P. Ronchi[b], A.T.M. Lenferink[c], C. Tresoldi[b], C. Morasso[a], D. Mehn[a], M. Bedoni[a], S. Picciolini[a], L. W. M. M. Terstappen[c], F. Ciceri[b], C. Otto[c†], F. Gramatica[a†].

In the clinical practice, the diagnosis and classification of acute myeloid leukaemia (AML) and myelodysplastic syndrome (MDS) start from the manual examination of stained smears of bone marrow (BM) and peripheral blood (PB) by using an optical microscope. This step is subjective and scarcely reproducible. Therefore, the development of subjective and potentially automatable methods for the recognition of typical AML/MDS cells is necessary. Here we used Raman spectroscopy for distinguishing myeloblasts, promyelocytes, abnormal promyelocytes and erythrocytes, which have to be counted for a correct diagnosis and morphological classification of AML and MDS. BM samples from patients affected by four different AML subtypes, mostly characterized by the presence of the four subpopulations selected for this study, were analyzed. First, each cell was scanned by acquiring 4096 spectra thus obtaining Raman images which demonstrate an accurate description of morphological features characteristic of each subpopulation. Raman imaging coupled with hierarchical cluster analysis permitted the automatic discrimination and localization of nucleus, cytoplasm, myeloperoxidase containing granules and haemoglobin. Second, the averaged Raman fingerprint of each cell was analysed by multivariate analysis (principal component analysis and linear discriminant analysis) in order to study the typical vibrational features of each subpopulation and for the automatic recognition of cells. The leave-one-out cross validation of a Raman-based classification model demonstrated the correct classification of myeloblasts, promyelocytes (normal/abnormal) and erythrocytes with an accuracy of 100%. Normal and abnormal promyelocytes were distinguished with 95% accuracy. The overall classification accuracy considering the four subpopulations was 98%. This proof-of-concept study shows that Raman micro-spectroscopy could be a valid approach for developing label-free, objective and automatic methods for the morphological classification and count of cells from AML/MDS patients, in substitution of the manual examination of BM and PB stained smears.

Introduction

AML is the result of an abnormal proliferation and differentiation of hematopoietic cells in the bone marrow and is the most common leukaemia in adults.[1,2]

[a]Laboratory of Nanomedicine and Clinical Biophotonics, Fond. Don Carlo Gnocchi ONLUS, Piazzale Morandi 6, 20121, Milan, Italy; [b]Hematology and Bone Marrow Transplantation Unit, San Raffaele Scientific Institute, via Olgettina 58, 20132, Milan, Italy; [c]Medical Cell Bio Physics, MIRA Institute for Biomedical Technology and Technical Medicine, University of Twente; Dienstweg 1, 7522ND, Enschede, The Netherlands. E-mail: rvanna@dongnocchi.it.

If not recognized and treated, it causes a fatal outcome in weeks or months. MDS, which refers to a group of disorders characterized by an ineffective haematopoiesis, progresses to AML in about 30% of cases.[3] An accurate and objective diagnosis and classification of these two related disorders is extremely important to establish prognosis and treatments. The world health organization (WHO) classified MDS and different AML subtypes on the basis of clinical, morphologic, immunophenotypic and genetic features.[4] Although genetic abnormalities are nowadays good prognostic and therapeutic indicators, the morphological evaluation is still the first diagnostic step and remains of great importance for the diagnosis and classification of AML, and could be essential for

predicting the likelihood of MDS to transform in AML.[5] The morphological assessment includes the differential recognition and count of blasts (hematopoietic progenitor cells) and of other cell subpopulations at different differentiation stages (e.g. promyelocytes, erythroblasts, monoblasts) by examining manually at least 500 and 200 cells from bone marrow (BM) and peripheral blood (PB) stained smears, respectively. The count of >20% of blasts in BM and PB is the requisite threshold recommended for the diagnosis of AML, where the number of blasts for the diagnosis of MDS is between 5% and 20%. In addition, the different percentages and ratio between different cells (in particular: myeloblasts, promyelocytes, erythroblasts) is used for classifying different AML and MDS subtypes. Despite its importance, the count and recognition of these cells is still performed using an optical microscope. This procedure is therefore highly subjective, scarcely reproducible, error-prone, time consuming and cannot be substituted by the automatic flow cytometry analysis according to the most recent guidelines[4,6]. In addition, the confirmation of the subpopulation identity needs sometimes to be confirmed by cytochemistry (e.g. by using myeloperoxidase (MPO), nonspecific esterase (NSE), periodic acid-Schiff (PAS) stains). For these reasons new methods are needed for a more reproducible, objective, accurate and potentially automatable morphological assessment of AML and MDS.

Several advantages of using Raman spectroscopy for diagnosis have been already proven, including its chemical specificity that could potentially substitute traditional diagnostic methods based on the visual examination of histological specimens[7–12] (reviewed in ref.[13]). In particular, Chan and collaborators recently used Raman spectroscopy to study different cellular populations in acute lymphoblastic leukaemia (ALL) patients.[7] Here we report the first Raman-based characterization of cells from AML patients. We characterized myeloblasts, promyelocytes and erythroblasts, which must be recognized and counted for the diagnosis of both AML and MDS. Myeloblasts (or "blasts") are the less mature and less differentiate cells of the myeloid (granulocytic) lineage, with a high nucleocytoplasmatic ratio and without cytoplasmatic granules; promyelocytes are maturing cells in the myeloid lineage which are principally characterized by granules mainly containing MPO, by a central or eccentric nucleus and by a reduced nucleocytoplasmatic ratio; erythroblasts are the nucleated precursors of erythrocytes, which start to express haemoglobin in the cytoplasm. In addition, we also studied abnormal promyelocytes which can be distinguished from normal promyelocytes (which we refer to here as "promyelocytes") mainly because of the hypergranularity of the cytoplasm, which commonly presents clumps of granules also called Auer rods[14]. Consequently, we used bone marrow samples from patients affected by four AML subtypes because mainly characterized and enriched by the four subpopulations selected. In details, "AML with minimal differentiation" (or "AML M0" according the French American Britannic (FAB) morphological classification[14,15]) was selected for studying myeloblasts; "AML with t(8;21); RUNX1-RUNX1T1" (or "AML M2") for

studying promyelocytes; "acute promyelocytic leukaemia (APL) with t(15;17); PML-RARA" (or "AML M3") for studying abnormal promyelocytes and "acute erythroid leukaemia" (or "AML M6") for studying erythroblasts. Firstly, we approached with Raman imaging for describing the morphology of the four selected subpopulations after having considered the excellent results recently obtained by using Raman imaging of cells.[16–20] Indeed, whereas for studying ALL, Chan and collaborators acquired a single Raman spectra of the nucleus of lymphoblasts[7], which are basically characterized by a prominent nucleus and a very small cytoplasm, we had to consider Raman imaging for studying AML and MDS cells which are generally larger, have a more complex morphology and are more heterogeneous if compared to ALL cells. For this purpose, we took advantage of a previously described home-built Raman setup that enable high-speed and high-quality chemical imaging[19,21]. In addition, we considered advantageous the use of a laser excitation at 647.1 nm for the analysis of hematopoietic cells. For instance, the excitation at 647.1 nm can induce a discrete pre-resonant enhancement of some vibrational modes of heme-containing proteins, in particular MPO and HB, due to the weak (but not null) absorption of the heme group in the region between 600 and 700 nm. At the same time, the 647.1 nm wavelength is far enough from frequencies with high absorbance (Soret band around 400 nm and other weak bands above 700 nm) thus avoiding strong resonance Raman scattering effects which could dominate the spectrum and completely mask Raman bands related to other important cellular components. After having characterized and compared the morphology of different cells by Raman imaging, we explored the possibility to discriminate these cells by using the single cell Raman fingerprint derived by averaging all the spectral information contained in the Raman image data-sets. This was done for verifying that a single acquisition of the whole cellular area, or a small number of acquisitions over the cell, could potentially permit the correct identification of different cells without the necessity of employing protocols of Raman imaging measurement, thus permitting the further development of faster and more feasible methods. A multivariate analysis approach, principal component analysis (PCA) coupled with linear discrimination analysis (LDA), was hence used for identifying significant spectral differences between cells and to build a classification model for automatically discriminating different cells typically counted for the assessment of AML and MDS.

Materials and methods

Patient samples and standard diagnostic procedure

The patients included in this study gave written informed consent in accordance with the protocols approved by the ethics committee of Hospital San Raffaele. The Patients' characteristics are listed in Supplementary Table S1. Different leukaemia subtypes were classified according to both the WHO classification[4,22] and FAB classification[23] by haematologists on

blood and marrow smears contextually with the routine diagnostic procedures. Morphological, immunophenotypical, cytogenetic and molecular genetics evaluations were performed following the most recent guidelines.[6] Histological bone marrow smear were stained using May-Grünwald-Giemsa (MGG) stain (Hemacolor - Merck).

Sample Preparation for Raman measurements

For each patient, a fraction of bone marrow aspirate utilized for the normal diagnostic procedures was processed for the isolation of bone marrow mononucleated cells by Ficoll-Hypaque (Pharmacia Biotech, Uppsala, Sweden) density gradient. This cell fraction was then frozen in fetal bovine serum (FBS) containing DMSO 10% and stored in liquid nitrogen containers at -196°C till its use (5 x 10^6 cells/ml, final concentration). Before Raman measurements, cells were thawed at 37°C, resuspended in 10 ml of warm RPMI-1640 medium supplemented with 10% fetal bovine serum, washed once by centrifugation, re-suspended in 10 ml of PBS medium and resuspended in PBS to reach a concentration of 1 x 10^6/ml. All cell preparations were >90% viable as assessed by trypan blue dye exclusion. Meanwhile, 20 mm diameter calcium fluoride (CaF_2) discs (Crystran LTD, Poole, UK), used as optical substrates for Raman measurements, were incubated with 0.01% poly-L-lysine for 30 min at 37°C to enable cell adhesion. Around 9 x 10^5 cells were then deposited on the CaF_2 discs by incubation at 37°C for 20 min. Subsequently the discs were rinsed three times with warm PBS. Immediately after the cells were fixed for 30 min at 37°C with 2 vol.% paraformaldehyde-PBS solution to avoid stress, activation and differentiation of cells. Before Raman measurements, the CaF_2 with immobilized cells was washed three times and immersed in PBS. At the same time, part of the same suspension (5 x 10^5 cells) was carefully cytospinned on glass slides and stained using May-Grünwald-Giemsa.

Raman Microspectroscopy

For Raman measurements a home-built confocal Raman microspectrometer was used as recently described.[19,21] Briefly, a Kr ion laser (Coherent, Innova 70C-Spectrum, Santa Clara, CA, USA) at the wavelength of 647.1 nm was filtered with a band-pass filter (Z647BP, Chroma Technology, Rockingham, VT, USA) and then reflected by a dichroic beam splitter (Z647RDC, Chroma Technology) to separate excitation and emission photons. The light was then focused on the sample by an immersion objective (63x/1.0 NA, W-Plan-Apochromat, Carl Zeiss, Jena, Germany). The scattered photons were then collected by the same objective, transmitted by the dichroic beam splitter and filtered with a razor-edge long-pass filter (LP02-647RU, Semrock, Buffalo, NY, USA) to remove the laser light. The scattered light was focused by a lens (f = 30 mm, AC127-030-B, Thor Labs, Newton, NJ, USA) on a confocal pinhole with a diameter of 15 μm at the entrance of the spectrograph. The final magnification of the light on the pinhole was 23x with a spatial resolution of ~390 nm (full width half maximum (FWHM)), which corresponds to the laser

spot size, and an axial resolution of around 1400 nm.. A thermoelectrically cooled electron multiplying charge-coupled device (EMCCD) chip (1600 x 200 pixels) (Newton DU-970N, Andor Technology, Belfast, Northern Ireland) was used as detector. A spectral range of around 3600 cm^{-1} and an average spectral resolution of 2.25 cm^{-1} was then obtained. Each cell was scanned by 64 x 64 (4096) Raman spectra over the entire cell area by a scanning mirror (Leica Laser Technique, GmbH, Heildelberg, Germany). The lateral dimension of the scanned cell area was between 10.0 to 14.0 μm, depending to the measured cell, corresponding to a step size of 156 to 218 nm, respectively.. The excitation power measured at the level of the sample was 36 mW and each spectrum was obtained with an acquisition time of 100 ms. The focus of the light, adjusted in order to get the higher signal from the cell, was positioned between 4 - 7 μm above the surface of the optical substrate depending on the dimensions of the cell.

Data Pre-processing

All data manipulation were performed using Origin (OriginLab, Northampton, MA) and custom software written with MATLAB 8.0 (The Math Works Inc., Natick, MA) and LabView (National Instruments Corp., Austin, TX). All spectra were pre-processed by removal of cosmic rays, subtraction of the camera offset, calibration of the wavenumber axis and correction of wavenumber-dependend transmission as described previously.[19] Toluene and argon light source bands were used to calibrate the setup. The detection efficiency at different wavelength and the detector induced etaloning were corrected using a tungsten halogen light source with a known emission spectrum (Avalight-HAL; Avantes BV, Eerbeek, The Netherlands). Singular value decomposition (SVD) was used to reduce the spectral noise.

Raman Imaging

For hierarchical cluster analysis (HCA) Raman imaging,[21] each dataset (4096 spectra matrix) derived from a singular cell was analyzed by HCA and principal component analysis (PCA) to automatically distinguish regions of the scanned area with different Raman features. In the cluster analysis routine, PCA scores were taken as input variables, squared Euclidean distances were used as distance measure, and Ward's algorithm was used to partition Raman spectra into clusters. Eight to ten level of HCA clustering, depending on cellular dimensions and complexity, were used in order to obtain HCA Raman images with a good description of the subcellular composition. Each cluster was assigned to a different colour thus obtaining a false-colour image of the cell on the basis of similar spectral features. For each cell, all spectra described for each cluster were averaged to obtain the mean cluster spectra. Each mean cluster spectra was then corrected subtracting the mean spectra of the background measured around the cell, mostly corresponding to the buffer and to the poly-lysine treated CaF_2 surface. Multivariate Raman images were produced overlapping different univariate images derived by the integration of a specific Raman band after subtraction of the local baseline. A

properly selected Raman band represents a known chemical compound, and its spatial distribution is represented by a single colour from the RGB pallet of the RGB image. The intensity of the colour is determined by the integrated intensity of the selected Raman band. In this way a combination of 3 compounds (or cellular components) can be represented in a single RGB-colour image. Multivariate Raman images were produced overlapping different univariate images derived by the integration of a specific band after subtraction of the local baseline.

Statistical and Multivariate Analysis

Single cell fingerprints utilized for comparing different cells and patients were obtained by utilizing a two-level HCA, selecting the cluster corresponding to the cell area, and by the subtraction of the cluster spectrum associated to the background. All cell fingerprint spectra were vector normalized in the range of 600-1750 cm^{-1} for further analyses. All cell fingerprint spectra of the same patient, and those belonging to the same AML subtype, were averaged thus obtaining the patient fingerprint spectra and the AML subtype fingerprint spectra, respectively. PCA was performed on the whole dataset in order to reduce the complexity of Raman spectra and to compare all cells from different AML subtype against each other. In order to perform PCA, all single cell fingerprints were baseline corrected by second-order polynomial fitting in order to eliminate eventual fluorescence components. All spectra were analyzed utilizing a variance-covariance matrix. The complexity of the original data was reduced by PCA producing 58 principal components (PCs). The first two PCs, which account for >87% of the variance, were then used to build the PCA scatter plot. A linear discriminant analysis (LDA) classification model was built using as training data the first eight PCs, which together describe >98% of the variance of the complete dataset, using the four AML subpopulation as different groups and setting prior probabilities proportional to the group size. The PCA-LDA classification model was validated by leave-one-out cross validation using functions of Origin (OriginLab, Northampton, MA). By using this method, for each cell (test data), the PCA-LDA model was built using all the remaining cells (training group) and then used to classify the test cell. This procedure was repeated until all cells were predicted once, thus defining the prediction accuracy of the model.

Results

High-resolution Raman imaging

High-resolution Raman images were obtained from cells isolated form BM aspirate of seven patients affected by different AML subtypes (details in Table 1). Each BM aspirate sample was evaluated during the routine diagnostic procedures and classified according to both the WHO[4,22] and FAB classification[23,14] considering all available information: clinical

Patient n.	AML subtypes (WHO classification)	characteristic AML subpopulation	AML Morphologic Subtype (FAB)*
1	AML with minimal differentiation	myeloblasts	M0
2	AML with minimal differentiation		
3	AML with t(8;21) ; RUNX1-RUNX1T1	promyelocytes	M2
4	AML with t(8;21) ; RUNX1-RUNX1T1		
5	APL with t(15;17); PML-RARA	abnormal promyelocytes	M3
6	APL with t(15;17); PML-RARA		
7	Acute erythroid leukaemia	erythroblasts	M6

Table 1 Patients selected in this study. *FAB subtypes names, M0: "AML with minimal evidence of myeloid differentiation"; M2: "AML with maturation"; M3: "Acute hypergranular promyelocytic leukaemia"; M6: "AML with predominant erythroid differentiation"

features, morphology, cytochemistry, immunophenotype, conventional and molecular cytogenetics, and molecular genetics (See Table S1 for details). Each cell was then selected by morphological criteria according to FAB and WHO guidelines. Myeloblasts (n=17) were analyzed from two patients affected by "AML with minimal differentiation"; promyelocytes (n=21) were analysed from two patients affected by "AML with t(8;21)(q22;q22); RUNX1-RUNX1T1"; abnormal promyelocytes (n=13) from two patients affected by "APL with t(15;17)(q22;q12); PML-RARA" and erythroblasts (n=8) from a single patient affected by "acute erythroid leukaemia" in clinical remission. After spectra pre-processing, Raman images were produced by HCA in the spectral range between 500-1800 cm^{-1} in order to automatically distinguish cell boundaries and different components of the cell at subcellular level. Fig. 1 shows the high correspondence between the cellular morphology observed by the optical microscope and corresponding HCA Raman images (Fig. 1i-l). Spectra related to different clusters are reported in Fig. 2a-d, ordered by relative overall intensity and respectively to the HCA images of Fig.1i-l. The detailed assignment of the most important Raman bands can be found in Table S2. By observing HCA images appears that cell boundaries, nucleus, cytoplasm, and some other morphological features are described by different clusters. Fig. 1i shows an example of HCA images of a myeloblasts from a patient affected by "AML with minimal differentiation". Here, the distribution of clusters indicates the regular shape of the nucleus (clusters from blue to green) with characteristic DNA-related bands (especially 788 and 1341 cm^{-1}) surrounded by a thin cytoplasmic region (red and cyan) related to cluster spectra without DNA-related vibrational bands (Fig. 2a,e). Moreover, the cluster distribution demonstrates an elevated nucleocytoplasmic ratio (>70% of the spectra recorded inside the cell) as typically observed by histological evaluation on stained samples (Fig. 1a). Likewise,
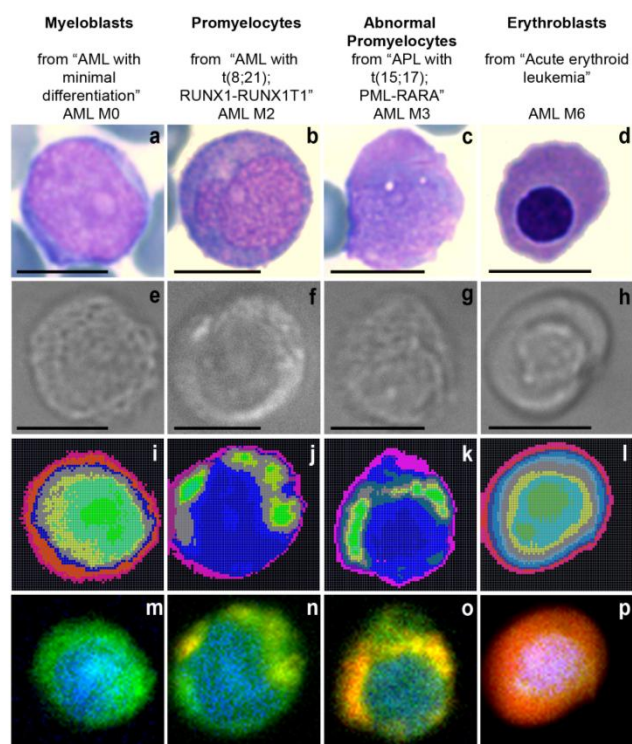
Fig. 1 Raman imaging of four different AML cells typical of the four AML subtypes analyzed. (a-d) Different AML cells stained with May-Grünwald-Giemsa stain; (e-h) bright field images of AML cells before the Raman measurement; (i-l) HCA images with colours corresponding to different cluster spectra showed in Fig.2a-d, respectively; (m-p) multivariate images derived by the selection of specific bands related to the nucleus (blue) and to the cytoplasm (green) for all images; the band related to MPO (red) was selected for creating images (m, n, o); the band related to haemoglobin (red) was selected for the image (p). In all multivariate images the green and the red pixels were overlapped (yellow) proportionally to the relative band intensities. Scale bars: 10 μm.

we created corresponding multivariate images (Fig. 1m) by selecting and integrating theDNA (nucleus) vibration band around 788 cm⁻¹ (blue) and the protein/lipids CH vibration (cytoplasm) around 1450 cm⁻¹ (green), demonstrating similar distribution and morphological features. In contrast, the HCA

images of promyelocytes from patients affected by "AML with t(8;21)(q22;q22); RUNX1-RUNX1T1" (Fig. 1j) show a smaller nuclear/cytoplasmic ratio (around 40%), high sub-cellular heterogeneity, an eccentric nucleus and the presence of granular-shaped clusters (grey, yellow, green) located specifically in the perinuclear region, absent in myeloblasts.. The spectra corresponding to these perinuclear clusters are very different from nucleus-related clusters (blue) and are characterized by intense bands located especially around 752, 1107, 1208, 1359 and 1582 cm⁻¹ (Fig. 2b,f). These Raman signals are corresponding to two heme groups of MPO (as confirmed by previous studies[24]), which is the most important marker of granulocytic (neutrophilic) differentiation and which is contained in granules (azurophilic granules) of promyelocytes. The distribution of MPO containing granules at subcellular level is also clearly shown in the multivariate image (Fig. 1n) obtained selecting the band around 1582 cm⁻¹ for MPO granules (representing around the 30% of the entire cellular area, red), around 788 cm⁻¹ (nucleic acid, blue) and around 1450 cm⁻¹ (cytoplasm, green). The HCA images and the multivariate images of an abnormal promyelocytes from patients affected by "APL with t(15;17); PML-RARA" (Fig. 1k,o) are similar to the Raman images of promyelocytes (Fig. 1j,n) but clearly show some typical abnormal features that characterize this type of AML cells. In fact, according to what observed by MGG staining (Fig. 1c), the Raman images demonstrate a smaller nucleocytoplasmic ratio (around 35%), an elongated shape, a more eccentric nucleus and a large portion of the cell (around 45%) characterized by very intense spectra related to the hypergranularity (MPO granules) described for abnormal promyelocytes[14]. HCA spectra of abnormal promyelocytes (Fig. 2c,g) have features similar to those derived from promyelocytes but with small differences better described by PCA results (see below). Figure 1l shows the HCA image derived from an erythroblast of a patient affected by acute erythroid leukaemia. The most prominent characteristic of HCA related spectra (Fig. 2d,h) is the contribution of bands relative to haemoglobin (in particular

Fig. 2 HCA results. (a-d) Background-free cluster spectra related to HCA images reported in Fig. 1.i (myeloblast), Fig 1.j (promyelocytes), Fig 1.k (abnormal promyelocytes) and Fig 1.l (erythroblasts), respectively; (e-h) selection of significant cluster spectra from images (a-d), respectively; for (e) and (h) the cytoplasm near the membrane cluster (pink) and the nucleus cluster (green) were selected and magnified; for (f) and (g), the nucleus cluster (blue) and the cytoplasmic granules (green) were selected and magnified. All spectra are shifted for clarity. Band assignments are reported in Table S2.
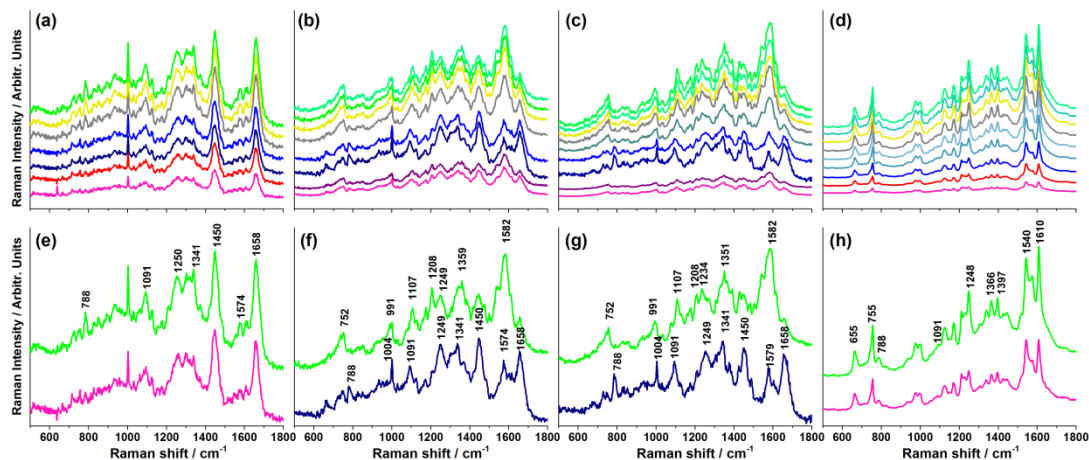
around 665, 755, 1249, 1173, 1249, 1366, 1397, 1540, 1610 cm^{-1})[25] over the entire cell area. HCA resulted in clusters very similar to each other with the exception of clusters located in the nuclear region of the cell (from grey to green) in which DNA bands (around 788 cm^{-1}) increase relatively to other bands. Similarly, the multivariate image (Fig. 1p) constructed selecting haemoglobin (red, 1610 cm^{-1}), DNA (blue, 788 cm^{-1}) and cytoplasm (green, 1448 cm^{-1}), shows that the cytoplasm is dominated by the presence of haemoglobin, even if the nucleus is clearly recognizable.

Identification of different subpopulations by individual cell average spectra

After having confirmed the potentialities of Raman imaging for the study of the morphology of cells that have to be recognized for assessing AML and MDS, we tested the capability of Raman spectroscopy to distinguish different types of cells by using the mean spectrum of each cell. The 4096 spectra collected from each cell were used to calculate the single-cell fingerprint by averaging all the spectra related to the cell area (calculated by a two-level HCA) and by subtracting the cluster spectrum associated to the background around the cell (mostly related to the buffer solution). Afterwards, all single-cell Raman fingerprints were used to calculate the average spectra (subpopulation fingerprint) (Fig. 3a-d) of myeloblasts, promyelocytes, abnormal promyelocytes and erythroblasts selected from different patients as described above. The standard deviation plotted along patient fingerprints (Fig. 3a-d) and the corresponding overall coefficient of variation (<5.5% for each mean spectrum) demonstrates a good reproducibility. However, the standard deviation of each subpopulation, plotted alone in Fig. S1a-d for clarity, shows that subtype fingerprints derived from promyelocytes and abnormal promyelocytes exhibit several bands with higher variance (especially between 1500 and 1650 cm^{-1}) than what observed in myeloblasts and erythroblasts. In general, myeloblasts exhibit intense variances mostly in correspondence of bands with high intensity, especially bands related to DNA (788 and 1375 cm^{-1}) proteins and lipids (1002, 1450 and 1658 cm^{-1}), reflecting differences in the nucleocytoplasmic ratio between different cells. Promyelocytes and abnormal promyelocytes show high variability in the region from 1500 and 1630 cm^{-1}, principally related to MPO, most likely due to the heterogeneity of myeloid granules and of their contents, which is very variable especially during the myeloid maturation.[26] For erythroblasts, the most intense variance is related to bands around 663 (porphyrin deformation) and 1609 (vinyl C=C stretch of deoxy-Hb) related to different amount of cytosolic haemoglobin.[27]

By observing Fig. 3a-d is clear that myeloblasts, promyelocytes (normal and abnormal considered together) and erythroblasts, are easily distinguishable by some typical spectral features in the region between 1500-1650 cm^{-1} and between 650-800 cm^{-1}. On the other hand, promyelocytes and abnormal promyelocytes are more similar and only some relevant differences are
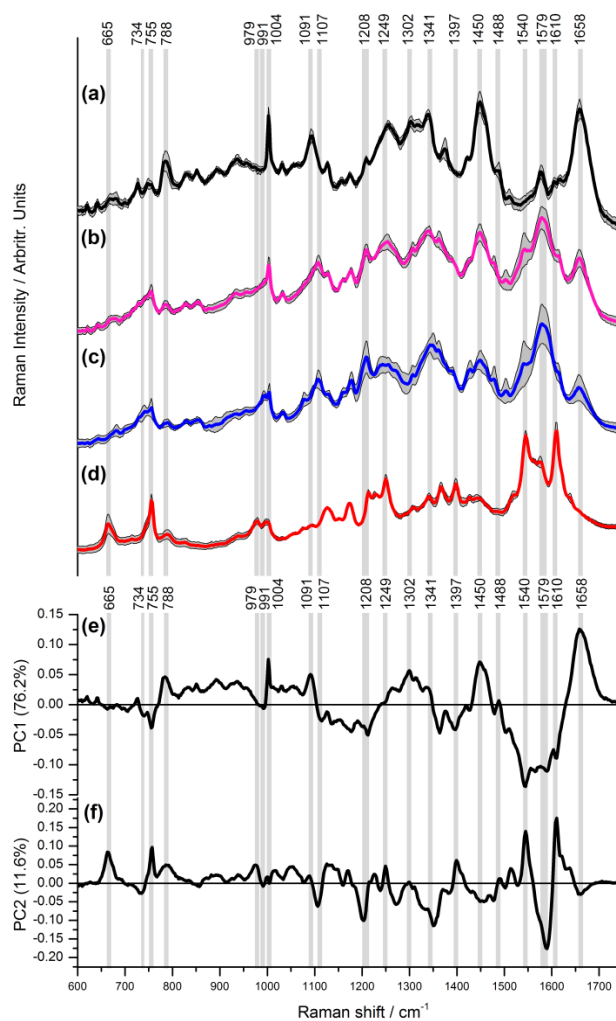

Fig. 3 Subpopulation fingerprints and PC loadings. Overall mean Raman spectra of: (a) myeloblasts from patients affected by "AML with minimal differentiation" (M0); (b) promyelocytes from patients affected by "AML with t(8;21) ; RUNX1-RUNX1T1" (M2); (c) abnormal promyelocytes from patients affected by "APL with t(15;17); PML-RARA" (M3); (d) erythroblasts from a patient affected by "Acute erythroid leukaemia" (M6). (e-f) two principal components (PC1 and PC2, respectively), representing together the 89.35% of the total variance, derived by PCA of the entire dataset. Gray bars indicate the most relevant Raman bands. All spectra are shifted for clarity.

distinguishable by simple observation: bands around 991, 1208 and 1450 cm^{-1} (Fig. 3b,c).Principal component analysis (PCA) was used to reduce the number of spectral variables in order to determine similarities/differences between cells and to allowing easy and automatic differentiation of the selected subpopulations. The first two principal components (PC1 and PC2)(PC loadings in Fig. 3e,f), which together define the 89.35% of the spectral variance between all spectra analyzed, were used to visually separate the cells in a bidimensional PCA scatter plot (Fig. 4). The first evidence is that, first, myeloblasts and erythroblasts are completely separated and distant from other cells; second, that they exhibit low dispersion indicating high homogeneity. Besides, promyelocytes and abnormal promyelocytes, even if distinguishable in two different groups by using more than two PCs (see linear discriminant analysis
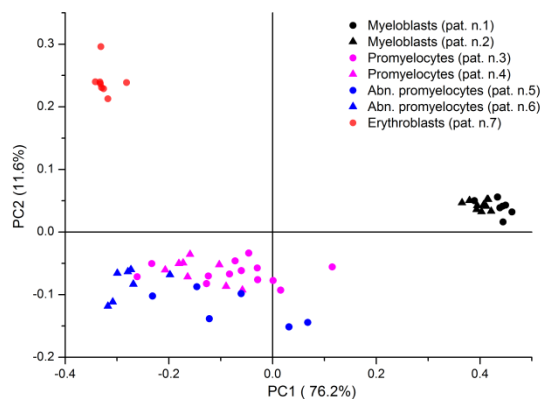
Fig. 4 PCA score plot of PC1 and PC2. (black) Myeloblasts from patients affected by "AML with minimal differentiation" (M0); (pink) promyelocytes from patients affected by "AML with t(8;21) ; RUNX1-RUNX1T1" (M2); (blu) abnormal promyelocytes from patients affected by "APL with t(15;17); PML-RARA" (M3); (red) erythroblasts from a patient affected by "Acute erythroid leukaemia" (M6).
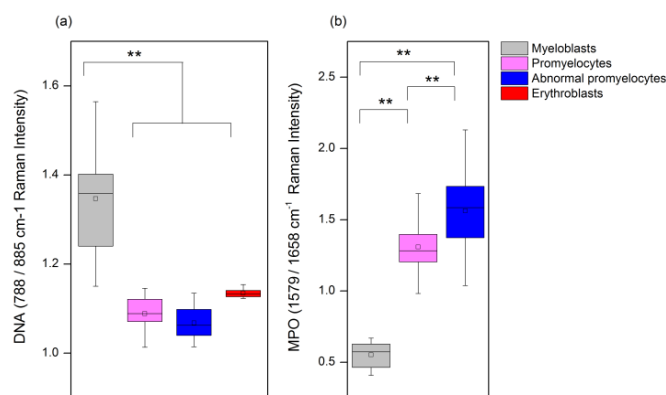

Fig. 5. Comparison of averaged intensity of DNA and MPO peaks in different subpopulations. (a) Box plot of averaged DNA peak intensity (ratio between DNA peak around 788 cm^{-1} and a baseline peak around 855 cm^{-1}) of myeloblasts from patients affected by "AML with minimal differentiation" (M0) (grey), promyelocytes from patients affected by "AML with t(8;21) ; RUNX1-RUNX1T1" (M2) (pink), abnormal promyelocytes from patients affected by "APL with t(15;17); PML-RARA" (M3) (blu), erythroblasts from a patient affected by "Acute erythroid leukaemia" (M6) (red). (b) box plot of the averaged MPO peak intensity (ratio between intensities of the MPO peak around 1579 cm^{-1} and the amide I peak at 1658 cm^{-1}) of myeloblasts (grey), promyelocytes (pink) and abnormal promyelocytes (blu). Boxes are defined by median, 25th and 75th percentile; whisker are min/max values, little squares are the mean. (**) Calculated p-value <0.01.

(LDA) below), are clustered in contiguous regions of this scatter plot, according to their similar condition of maturing cells in the granulocytic lineage, mostly characterized by an increased level of MPO and other granules-related proteins. Moreover, as mentioned above, the fact that these two groups are much more dispersed than myeloblasts and erythroblasts in the PCA scatter plot, confirm the relative high level of heterogeneity of these type of cells, mostly due to different level of dysplasia and maturation of each measured cell. The PC1 (loadings in Fig. 3e), which describe the 76.2% of variance of the entire dataset, mainly define differences between immature AML cells (myeloblasts) and the other three AML

subtypes characterized by maturation in the myeloid lineage (myeloblast, promyelocytes and erythroblasts). All myeloblasts are associated with high positive PC1 scores (right side of the plot in Fig. 4), promyelocytes, abnormal promyelocytes and erythroblasts are associated with low or negative scores of PC1 (left side of the plot in Fig. 4). On the other hand, PC2 (representing the 11.6% of the spectral variance) do not describe significant variations related to myeloblasts (PC2 scores near zero) but clearly discriminates erythroblasts (PC2 positive scores, upper-left of the plot in Fig. 4) and promyelocytes and abnormal promyelocytes (PC2 negative scores, bottom-left of the plot in Fig. 4). Then, promyelocytes and abnormal promyelocytes are distinguishable in two groups on the basis of different values of both PC1 and PC2 scores but especially because of PC2 contribution.

PCA, other than permitting to group together different cell types, helps in the comprehension of spectral features that differentiate these cells. The positive portion of the PC1-loadings spectrum (Fig. 3e) is basically characterized by bands around 788 cm^{-1} (O-P-O symmetric stretch and nucleic acid bases vibrations) and 1091 cm^{-1} (O-P-O symmetric stretch), related to the DNA, by bands around 1004 cm^{-1} (phenylalanine) and 1660 cm^{-1} (amide I band), assigned to proteins, and the band around 1450 cm^{-1} (C-H deformation bands) generally assigned to proteins, lipids and carbohydrates. In summary, these features are in accordance with the immature stage of myeloblasts, characterized by a high nucleocytoplasmic ratio and by the absence of the expression of typical myeloid enzymes. The negative part of the PC1-loadings spectrum (Fig. 3e) mostly represents bands that are more intense in promyelocytes, abnormal promyelocytes and erythroblasts if compared to myeloblasts: especially around 755 and 991 cm^{-1}, and in regions between 1110-1250 cm^{-1}, 1350-1440 cm^{-1} and 1500-1630 cm^{-1}, all related to maturation (see below). However, the majority of these bands are then splitted in the two directions (positive and negative scores) of the PC2 loadings spectrum (Fig. 3f) and better describe spectral features responsible for the separation of erythroblasts (positive PC2 scores) and promyelocytes/abnormal promyelocytes (negative PC2 scores). Positive PC2 (erythroblasts) loadings show intense bands around 663, 755, 979, 1249, 1397, 1540 and 1610 cm^{-1}, related to haemoglobin.[25] Negative PC2 loadings (promyelocytes/abnormal promyelocytes) are principally positioned around 734, 1107, 1208, 1348, 1579 cm^{-1} and are mostly related to MPO.[24] Finally, as mentioned before, the most discriminant spectral features that differentiate promyelocytes and abnormal promyelocytes are the different intensities of the PC2 loadings spectra (Fig. 3f). Indeed, the PC2 loadings scores are generally more negative for abnormal promyelocytes cells thus indicating a higher contribution of MPO signal in these cells. The capability to quantitatively evaluate the relative abundance of indicative molecules using only Raman spectroscopy was also demonstrated by integrating the signals related to DNA and MPO bands (Fig. 5a). The mean normalized value of the DNA peak (788 cm^{-1}) is significantly

		Predicted				
		Myelo blasts	Promyelo cytes	Abn. promyelo cytes	Erythro blasts	Total true	Accura cy
True	Myelo blasts	17 (100% 100%)	0	0	0	17	100%
	Promyelo cytes	0	20 (95.3%, 95.1%)	1	0	21	96%
	Abn. promyelo cytes	0	2	11 (84.6%, 98.0%)	0	13	96%
	Erythro-blasts	0	0	0	8 (100%, 100%)	8	100%
						59	98%

Table 2 Confusion table resulted from LDA based on PCA. In parenthesis sensitivity and specificity, respectively.

much higher (p < 0.01) in myeloblasts than in other cells. This is in agreement with the large portion of cell occupied by the nucleus in immature cells. The mean normalized intensity of peaks related to MPO (1579 cm^{-1}) (Fig. 5b) significantly demonstrates differences between myeloblasts, promyelocytes and abnormal promyelocytes (erythroblasts were excluded because they do not express MPO).

Despite the analysis of the first two PCs is very useful for a visual discrimination of different cells and to understand which spectral features are typical of different cells, PCA-LDA classification has been employed as cross-validated unsupervisioned method to evaluate the accuracy of the Raman-based method. A PCA-LDA classification model was build considering the first 8 PCs (corresponding to the 97.7% of the variance of the dataset) as input variables and was then cross-validated by leave-one-out cross validation. The PCA-LDA model obtained demonstrated that Raman spectroscopy was able to accurately classify the cells in the four distinct subpopulations as showed in Table 2. All myeloblasts and erythrocytes were correctly classified giving 100% accuracy, specificity and sensitivity. Similarly, promyelocytes (both normal and abnormal) were efficiently discriminated by myeloblasts and erythrocytes with 100% accuracy. Considering the differentiation between promyelocytes, one of 21 promyelocytes was wrongly classified as abnormal promyelocytes, giving 95% of sensitivity, 95% of specificity and 95% of accuracy; besides, out of 13 abnormal promyelocytes, two were misclassified as promyelocytes, resulting in 85% of sensitivity, 98% of specificity and 95% of accuracy for this class. Considering the four distinct subpopulations, the PCA-LDA classification model demonstrated overall 98% accuracy thus proving that myeloblasts, promyelocytes, abnormal promyelocytes and erythroblasts are distinguishable by Raman spectroscopy.

Discussion

Here we reported the characterization of cells which are usually evaluated by haematopathologists for the diagnosis of AML and MDS by means of Raman microspectrometry. Recent studies already reported the Raman-based differentiation of haematopoietic cells (e.g. Ramoji et al. distinguished normal neutrophils from normal lymphocytes with 97% accuracy and also reported the spectra of other nucleated cells, namely, eosinophils and monocytes;[28] Chan et al. characterized and distinguished T- and B-lymphocytes from patients affected by acute lymphoblastic leukaemia (ALL)[7]; Neugebauer et al. studied and separated cultured AML cells (OCI-AML) from other cancer cells in culture and normal cells from human blood[9] but, as far as we know, this is the first study of different typical AML/MDS cells from patients.

A Raman-based imaging method was utilized as first approach. The results showed that from the dataset derived from each scanned cell is possible to extract a large quantity of information which can be potentially analyzed in several ways. We showed that the hierarchical clusterization of data (HCA) permitted to automatically discriminate and to automatically localize different cellular components o molecules fundamental for differentiating haematopoietic cells (e.g. nucleus, cytoplasm, MPO containing granules, HB). This is significant if the objectivity and reproducibility of using a Raman-based method is compared to the manual evaluation of BM/BM smear at the microscope, and this is even more important if we consider the difficulties to objectively quantify immunohistochemistry[29]. In addition, we showed that by selecting a known spectral feature related to a molecule or a cellular component of interest, is possible to obtain fluorescence-like false-colour multivariate images. Here we clearly showed, for example, the ease evaluation of MPO signals, which were totally absent in myeloblasts, more evident in granular myeloblasts and very strong and diffuse in abnormal promyelocytes. If compared to traditional immunohisto-chemistry or immunofluorescence, this Raman-based approach, other than being a label-free method, permits to identify, localize and compare an indefinite number of molecules (or class of molecules) as much as are the number of specific features detectable by Raman spectroscopy. For this study we have chosen to start from getting a large amount of information by the acquisition of a very high number of spectra (4096) from each cell, thus resulting in a relatively long measurement time (around 6.8 minutes). We followed this strategy for obtaining an exhaustive characterization of the cells in prospective to further explore and develop faster and more feasible acquisition method like line mapping technique, wild field Raman imaging,[30] and two-dimensional fast Raman imaging (DuoScan).[31] The data obtained in this study will be helpful for knowing both the cellular positions to be preferentially assessed in the case of line mapping technique, and the wavenumber range(s) that can be specifically monitored (e.g. bands related to MPO and DNA which change significantly between cells as demonstrated here).

Analyst Accepted Manuscript

In order to test the possibility to maintain specificity even reducing the information derived by high-resolution Raman imaging, we virtually eliminated the spatial information by averaging all the imaging spectral data in a single Raman fingerprint for each cell. PCA was used for demonstrating that the single cell fingerprint is still highly specific and for describing which spectral features can discriminate the different cells studied here. Subsequently, a classification model based on LDA showed that the PCs obtained from Raman data are able to distinguish myeloblasts versus promyelocytes (normal or abnormal) versus erythroblasts with 100% accuracy. A study by the International Working Group on Morphology of Myelodysplastic Syndrome (IWGM-MDS), reported the results of the manual examination of the same BM sample (from a patient affected by "AML with t(8;21) ; RUNX1-RUNX1T1" (M2)) by different expert haematopathologists for evaluating the reproducibility in distinguishing myeloblasts, promyelocytes and mature cells. As result, the IWGM-MDS reported percent of agreement from 72% to 85% thus showing that is not obvious the manual designation of the correct cell type and the reproducibility of this evaluation, and confirming the potentialities of using Raman spectroscopy in this field. In addition, we tested the capability of Raman spectroscopy of distinguishing promyelocytes from abnormal promyelocyte. Normally, the assessment of these cells by visual examination may be arduous because morphological criteria are vague and difficult to be objective: abnormal features refer mainly to hypergranularity and irregular distribution of granules, commonly aggregated in cytoplasmic clumps. For this purpose, we selected two patients affected by "APL with t(15;17); PML-RARA" (AML M3), with characteristic genetic abnormalities (i.e. the chromosomal translocation involving the gens PML and RARA) that induce the predominance of abnormal promyelocytes in BM and PB. Our Raman-based method succeeded in distinguishing normal and abnormal promyelocytes with an overall 95% of accuracy. This result is considerable especially taking in account that once acute promyelocytic leukaemia (AML M3) is suspected by the morphological evaluation, the disease should be managed as medical emergency with a specific treatment (all-trans retinoic acid) in the same day without waiting for genetic confirmation of the diagnosis.[32]

Finally, this study confirms that the use of the 647.1 nm excitation light (or similar) is appropriate for studying haematopoietic cells. In fact, the pre-resonance effects observed measuring cells containing MPO or HB, due to their weak adsorption around 600-700 nm, resulted to be very useful for a facile detection of these molecules without precluding the detection of other important cellular Raman signals (e.g. DNA, protein, lipids).

Conclusion

The exceptional compatibility of Raman spectroscopy with a relatively simple and highly informative diagnostic procedure based on the direct label-free measurement of patient specimens is confirmed by this study which report the capacity of Raman spectroscopy to characterize and assess typical cells of haematopoietic tumours. Here we have shown, even though at a proof of concept level, that different BM cells which usually have to be manually recognized and counted for the diagnosis and classification of AML and MDS, can be objectively and accurately discriminated by Raman spectroscopy. In particular, the high accuracy (100%) of the method reported here for distinguishing blasts from other AML/MDS cells (promyelocytes and erythrocytes) is very promising considering that the blast count in BM and PB is still nowadays the first essential step of the diagnosis and classification of AML and MDS. These results suggests that further studies and technological improvement of the acquisition techniques could pave the road to the development of Raman-based method for the automatic, objective and high-throughput definition and count of BM/PB cells for the assessment of AML and MDS.

Acknowledgements

References

1   E. Estey and H. Döhner, *The Lancet*, 2006, **368**, 1894–1907.

2   B. Deschler and M. Lübbert, *Cancer*, 2006, **107**, 2099–2107.

3   A. F. List, J. Vardiman, J.-P. J. Issa and T. M. DeWitte, *ASH Educ. Program Book*, 2004, **2004**, 297–317.

4   J. W. Vardiman, J. Thiele, D. A. Arber, R. D. Brunning, M. J. Borowitz, A. Porwit, N. L. Harris, M. M. L. Beau, E. Hellström-Lindberg, A. Tefferi and C. D. Bloomfield, *Blood*, 2009, **114**, 937–951.

5   G. J. Mufti, J. M. Bennett, J. Goasguen, B. J. Bain, I. Baumann, R. Brunning, M. Cazzola, P. Fenaux, U. Germing, E. Hellström-Lindberg, I. Jinnai, A. Manabe, A. Matsuda, C. M. Niemeyer, G. Sanz, M. Tomonaga, T. Vallespi and A. Yoshimi, *Haematologica*, 2008, **93**, 1712–1717.

6   H. Döhner, E. H. Estey, S. Amadori, F. R. Appelbaum, T. Büchner, A. K. Burnett, H. Dombret, P. Fenaux, D. Grimwade, R. A. Larson, F. Lo-Coco, T. Naoe, D. Niederwieser, G. J. Ossenkoppele, M. A. Sanz, J. Sierra, M. S. Tallman, B. Löwenberg and C. D. Bloomfield, *Blood*, 2010, **115**, 453–474.

7   J. W. Chan, D. S. Taylor, S. M. Lane, T. Zwerdling, J. Tuscano and T. Huser, *Anal. Chem.*, 2008, **80**, 2180–2187.

8   E. M. Kanter, E. Vargis, S. Majumder, M. D. Keller, E. Woeste, G. G. Rao and A. Mahadevan-Jansen, *J. Biophotonics*, 2009, **2**, 81–90.
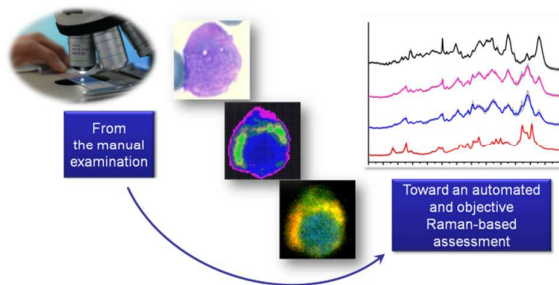
9   U. Neugebauer, T. Bocklitz, J. H. Clement, C. Krafft and J. Popp, *The Analyst*, 2010, **135**, 3178.

10 L. Hartsuiker, N. J. L. Zeijen, L. W. M. M. Terstappen and C. Otto, *The Analyst*, 2010, **135**, 3220–3226.

11 S. M. Ali, F. Bonnier, K. Ptasinski, H. Lambkin, K. Flynn, F. M. Lyng and H. J. Byrne, *The Analyst*, 2013, **138**, 3946–3956.

12 T. Minamikawa, Y. Harada, N. Koizumi, K. Okihara, K. Kamoi, A. Yanagisawa and T. Takamatsu, *Histochem. Cell Biol.*, 2013, **139**, 181–193.

13 S. Wachsmann-Hogiu, T. Weeks and T. Huser, *Curr. Opin. Biotechnol.*, 2009, **20**, 63–73.

14 B. J. Bain, *Leukaemia Diagnosis*, John Wiley & Sons, 2010.

15 J. M. Bennett, D. Catovsky, M. T. Daniel, G. Flandrin, D. A. Galton, H. R. Gralnick and C. Sultan, *Ann. Intern. Med.*, 1985, **103**, 620–625.

16 H.-J. van Manen, Y. M. Kraan, D. Roos and C. Otto, *Proc. Natl. Acad. Sci. U. S. A.*, 2005, **102**, 10159–10164.

17 C. Matthaus, T. Chernenko, J. A. Newmark, C. M. Warner and M. Diem, *Biophys. J.*, 2007, **93**, 668–673.

18 K. Hamada, K. Fujita, N. I. Smith, M. Kobayashi, Y. Inouye and S. Kawata, *J. Biomed. Opt.*, 2008, **13**, 044027–044027–4.

19 V. V. Pully, A. T. M. Lenferink and C. Otto, *J. Raman Spectrosc.*, 2011, **42**, 167–173.

20 K. Klein, A. M. Gigler, T. Aschenbrenner, R. Monetti, W. Bunk, F. Jamitzky, G. Morfill, R. W. Stark and J. Schlegel, *Biophys. J.*, 2012, **102**, 360–368.

21 V. V. Pully, A. Lenferink and C. Otto, *J. Raman Spectrosc.*, 2010, **41**, 599–608.

22 J. W. Vardiman, N. L. Harris and R. D. Brunning, *Blood*, 2002, **100**, 2292–2302.

23 J. M. Bennet, D. Catovsky, M. T. Daniel, G. Flandrin, D. A. G. Galton, H. R. Gralnick and C. Sultan, *Ann. Intern. Med.*, 1985, **103**, 620–625.

24 G. J. Puppels, H. S. Garritsen, G. M. Segers-Nolten, F. F. de Mul and J. Greve, *Biophys. J.*, 1991, **60**, 1046–1056.

25 B. R. Wood and D. McNaughton, *J. Raman Spectrosc.*, 2002, **33**, 517–523.

26 K. Arnljots, O. Sørensen, K. Lollike and N. Borregaard, *Leukemia*, 1998, **12**, 1789–1795.

27 H. Sato, S. Wada, Y. Ozaki and H. Tashiro, *Vib. Spectrosc.*, 2004, **34**, 149–156.

28 A. Ramoji, U. Neugebauer, T. Bocklitz, M. Foerster, M. Kiehntopf, M. Bauer and J. Popp, *Anal. Chem.*, 2012, **84**, 5335–5342.

29 M. Cregger, A. J. Berger and D. L. Rimm, *Arch. Pathol. Lab. Med.*, 2006, **130**, 1026–1030.

30 S. Schlücker, M. D. Schaeberle, S. W. Huffman and I. W. Levin, *Anal. Chem.*, 2003, **75**, 4312–4318.

31 G. Falgayrac, B. Cortet, O. Devos, J. Barbillat, V. Pansini, A. Cotten, G. Pasquier, H. Migaud and G. Penel, *Anal. Chem.*, 2012, **84**, 9116–9123.

32 M. A. Sanz, D. Grimwade, M. S. Tallman, B. Lowenberg, P. Fenaux, E. H. Estey, T. Naoe, E. Lengfelder, T. Büchner, H. Döhner, A. K. Burnett and F. Lo-Coco, *Blood*, 2009, **113**, 1875–1891.

Analyst Accepted Manuscript

1
2
3
4
5
6
7
8
9
10
11
12
13
14
15
16
17
18
19
20
21
22
23
24
25
26
27
28
29
30
31
32
33
34
35
36
37
38
39
40
41
42
43
44
45
46
47
48
49
50
51
52
53
54
55
56
57
58
59
60

Label-free imaging and identification of typical cells of acute myeloid leukaemia and myelodysplastic syndrome by Raman microspectroscopy

Table of Contents

Heamatopoietic cancer cells from patients were objectively and accurately recognized by high-resolution Raman imaging and by their characteristic Raman spectra

From the manual examination

Toward an automated and objective Raman-based assessment